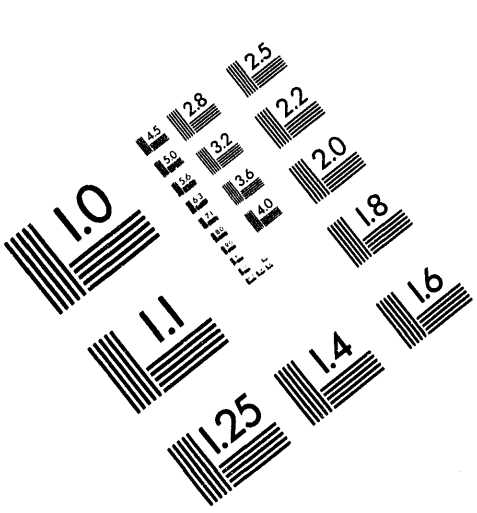

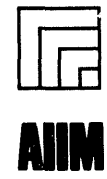

Association for Information and Image Management
1100 Wayne Avenue, Suite 1100
Silver Spring, Maryland 20910
301/587-8202

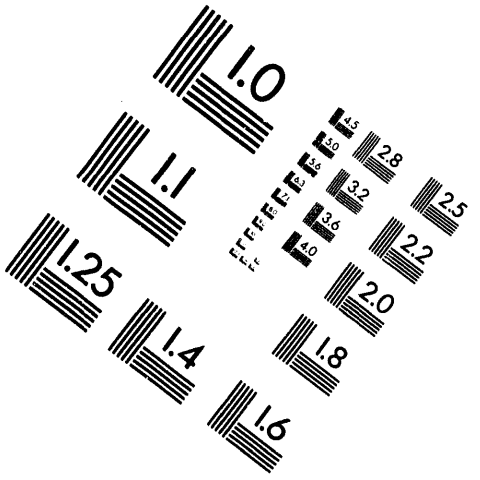

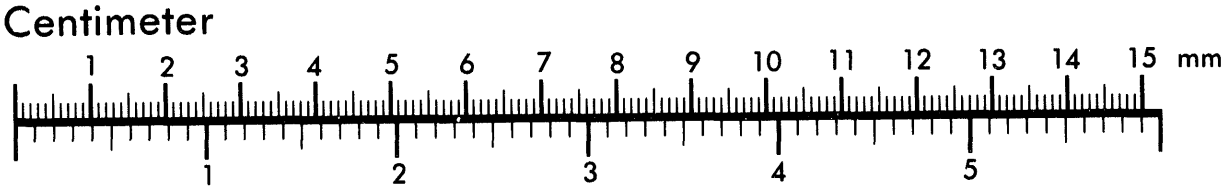

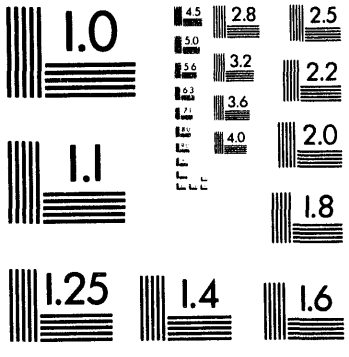

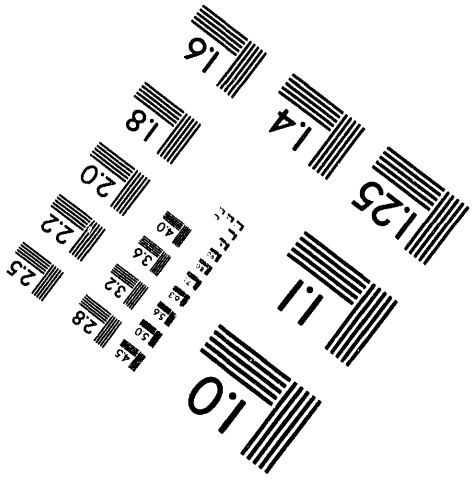

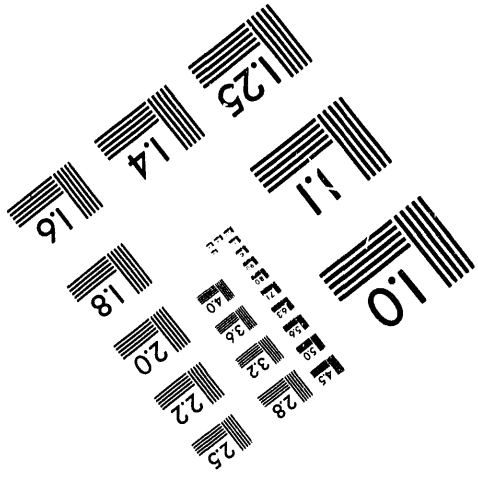

MANUFACTURED TO AIIM STANDARDS
BY APPLIED IMAGE, INC.

1 of 1

GA–A21742

A METHOD FOR MEASURING THE INDUCTIVE ELECTRIC FIELD PROFILE AND NONINDUCTIVE CURRENT PROFILES ON DIII–D

by

C.B. FOREST, K. KUPFER,* T.C. LUCE, P.A. POLITZER, L.L. LAO, and D. WROBLEWSKI†

This is a preprint of a paper to be presented at the 21st European Physical Society Conference on Controlled Fusion and Plasma Physics, June 27–July 1, 1994, Montpellier, France, and to be printed in the *Proceedings*.

Work supported by
U.S. Department of Energy
Contract Nos. DE-AC03-89ER51114 and W-7405-ENG-48

*ORISE Postdoctoral Fellow
†Lawrence Livermore National Laboratory

GENERAL ATOMICS PROJECT 3466
JULY 1994

GENERAL ATOMICS

A METHOD FOR MEASURING THE INDUCTIVE ELECTRIC FIELD PROFILE AND NONINDUCTIVE CURRENT PROFILES ON DIII-D*

C.B. FOREST, K. KUPFER†, T.C. LUCE, P.A. POLITZER, L.L. LAO, AND D. WROBLEWSKI‡

A new technique for determining the parallel electric field profile and noninductive current profile in tokamak plasmas has been developed and applied to two DIII-D tokamak discharges. Central to this technique is the determination of the current density profile, $J(\rho)$, and poloidal flux, $\psi(\rho)$, from equilibrium reconstructions.[1] From time sequences of the reconstructions, the flux surface averaged, parallel electric field can be estimated from appropriate derivatives of the poloidal flux. With a model for the conductivity and measurements of T_e and Z_{eff}, the noninductive fraction of the current can be determined. Such a technique gives the possibility of measuring directly the bootstrap current profile and the noninductively driven current from auxiliary heating such as neutral beam injection or fast wave current drive. Furthermore, if the noninductively driven current is small or if the noninductive current profile is assumed to be known, this measurement provides a local test of the conductivity model under various conditions.

TECHNIQUE

The noninductive current density can be determined from the equation relating the current density to the electric field,

$$\langle \vec{J} \cdot \vec{B} \rangle = \frac{1}{\eta} \langle \vec{E} \cdot \vec{B} \rangle + \langle \vec{J}_{NI} \cdot \vec{B} \rangle \quad , \tag{1}$$

if the current density and electric field are measured. In this equation, $\langle A \rangle$ is the flux surface average of A, η is the resistivity, and J_{NI} represents any sources of noninductive current drive (including both bootstrap current and auxiliary driven currents). The flux surface average of the quantity $\langle \vec{E} \cdot \vec{B} \rangle$ can be shown to be[2]

$$\langle \vec{E} \cdot \vec{B} \rangle = \frac{\langle B_\phi^2 \rangle}{F} \left. \frac{\partial \psi}{\partial t} \right|_\Phi \quad . \tag{2}$$

In this equation, the derivatives of poloidal flux ψ are taken on surfaces of constant toroidal flux, Φ; B_ϕ is the toroidal component of the magnetic field, and $F(\psi) = RB_\phi$. Thus the electric field is related solely to changes in poloidal flux, while the flux surface label Φ provides a proper reference frame in which no poloidal electric fields are induced from changes in toroidal flux. It is convenient to define an effective parallel electric field $\mathcal{E}_\parallel(\rho) = \langle \vec{E} \cdot \vec{B} \rangle / B_{t0}$ and current densities $J = \langle \vec{J} \cdot \vec{B} \rangle / B_{t0}$. In addition, the flux surface label, ρ, defined as $\sqrt{\Phi / B_{t0} \pi}$ is used rather than Φ, where B_{t0} is the vacuum field at the center of the vessel (R_0), and ρ has units of length.

To calculate $\mathcal{E}_\parallel$ for non-circular plasmas, the current density profiles and $\psi(R, Z)$ are first determined by fitting a solution of the Grad-Shafranov equation to measured quantities at several instances in time. Here, the code EFITD[3] is used. The reconstructions are constrained by measured values of the poloidal field and flux on the vacuum vessel wall, external coil currents, internal pitch angle measurements near the midplane of the tokamak, and measurements of electron and ion densities and temperature for the scalar pressure $p(\psi)$. As a result of the reconstructions, the quantities $q(\psi)$, $F(\psi)$, $B_\phi(R, Z)$ and $\psi(R, Z)$ are determined at each time

* Work was supported by the U.S. Department of Energy under Contract Nos. DE-AC03-89ER51114 and W-7405-ENG-48.

† ORISE Postdoctoral Fellow.

‡ Lawrence Livermore National Laboratory.

and $\psi(\rho)$ can be easily calculated [for example, from $q = (d\Phi/d\psi)$]. Once $\psi(\rho, t)$ is known for a time sequence of equilibria, then $\mathcal{E}_\parallel$ can be calculated from Eq. (2).

The inductive current $J_{oh}(\rho)$ is then calculated from a resistivity model (Spitzer conductivity or neoclassical conductivity[4]), which require accurate measurements of T_e and Z_{eff}. The profile of T_e is measured by Thomson scattering and electron cyclotron emmission (ECE). The carbon density (shown to be the predominant impurity by survey spectrometers) is determined by charge exchange recombination spectroscopy and used in combination with visible bremsstrahlung measurements to provide profiles of Z_{eff}. Typically, T_e is known with 5% accuracy, while Z_{eff} is known to 10%, predominantly due to uncertainties in the density profile. Finally, the noninductive portion of the current is the difference between $J_{oh}(\rho)$ and $J(\rho)$.

There are several considerations which restrict the applicability of this approach. First, the actual electric field may differ from the measured electric field if shorter time scale MHD fluctuations (*e.g.*, sawteeth) to the current profile exist. To see this, consider the actual poloidal flux to be a sum of a time averaged $\bar{\psi}$, averaged over the fluctuation period, and a fluctuating component $\tilde{\psi}$ due to the MHD activity. In general this fluctuating component could be measured, however the error introduced by taking derivatives on short time scales has only allowed measurements on a longer time scale. Second, this technique does not give the possibility of distinguishing between the various sources of noninductive current – it is only possible to determine the net noninductive current. Finally, if non-thermal electrons such as those produced by lower hybrid heating are present, the assumption of neoclassical resistivity may not be valid and the inductive current would be overestimated.

Uncertainties in the quantities $\mathcal{E}_\parallel$ [or $\psi(\rho, t)$] and $\langle \vec{J} \cdot \vec{B} \rangle$ are estimated by a Monte Carlo method in which each input datum to EFITD is randomly perturbed with a distribution characterized by the measurement's standard deviation and the equilibrium is recalculated many times. Such calculations show that the central current density is typically known with a 10% uncertainty, while the poloidal flux is known more accurately, with a 2% to 3% uncertainty. The uncertainty in calculating the inductive current is affected by uncertainties in the equilibria and by the measurements of Z_{eff} and $T_e^{3/2}$, which are also accounted for in this work.

RESULTS

Neoclassical conductivity is an adequate model to explain inductive current profiles in discharges without sawteeth. This is clearly demonstrated in a hot-ion L–mode[5] discharge with a current ramp. This plasma had 4.6 MW of neutral beam heating, with current ramp from 500 kA to 1.2 MA of 200 ms duration. The poloidal beta, β_p, changed from 1.4 before the current ramp to 0.3 following the current ramp, and thus little bootstrap current was expected during this slowly evolving phase following the current ramp (calculations show less than 20% noninductive). In addition, there was a 800 ms sawtooth free period following the current ramp during which the electric field profile was calculated from three equilibria (with a period of 200 ms starting 400 ms after the current ramp) without complications from fluctuating current profiles. The measured T_e and Z_{eff} profiles and the electric field profiles are shown in Fig. 1. The measured current profile $J(\rho)$ and the inductive current profiles calculated from neoclassical (J_{neo}) and Spitzer resistivity (J_{sp}) are also shown. The profiles of total current and neoclassical inductive current are similar in magnitude and shape. In contrast, Spitzer resistivity overestimates the current density by approximately a factor of two for much of the plasma. From this we assume that that the neoclassical resistivity model is sufficiently accurate for analyzing other discharges, in which the inductive current is a smaller fraction of the total current.

A similar technique applied to a discharge with sawteeth overestimates the inductive current in the sawtoothing region of the plasma. Figure 2 shows the measured current profile from a 2 MA, L–mode plasma with 6 MW of neutral beam heating and the inductive current density calculated from neoclassical conductivity. This result can be interpreted as an underestimate of

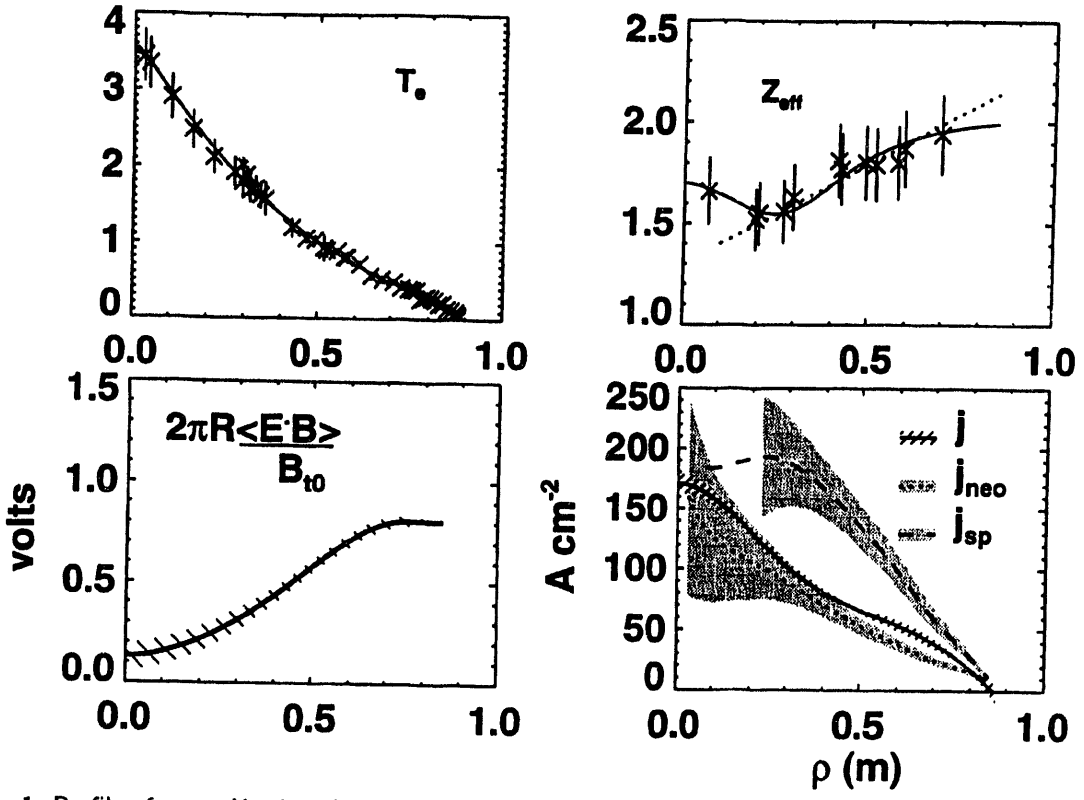

Fig. 1. Profiles from a Hot-ion, L–mode, with a large fraction of inductive current. The dotted line for Z_{eff} represents the result from visible bremsstrahlung. The inductive electric field is calculated by taking derivatives of poloidal flux from 3 equilibria spanning 400 ms. j is the measured current density, j_{neo} the result from neoclassical conductivity, and j_{sp} from Spitzer resistivity.

the resistivity, but this seems unlikely since we have already established that neoclassical resistivity is valid without sawteeth. It is more likely that a fluctuating component of the electric field due to the sawteeth subtracts from the measured electric field (which is averaged over many sawteeth periods) during the slowly evolving phase between each sawtooth crash.[6]

Resistive relaxation and broadening of the current profile has been observed in a high-β_p discharge. This plasma was an elongated ($\kappa = 2.1$), high triangularity ($\delta = 0.9$) shape, with a plasma current of 400 kA, and 8 MW of neutral beam heating. Following the start of beam injection, the current profile resistively relaxed as q_0 increased from ~1 at the beginning of beam injection, to >2, 2 seconds later. Figure 3 shows evolving profiles of ψ, j, and the loop voltage ($2\pi R\mathcal{E}$) during this evolving phase. As the current profile broadens, the

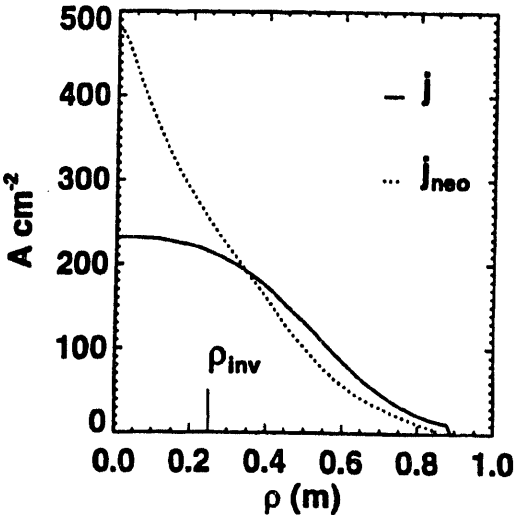

Fig. 2. Comparison of measured current profile and inductive current profiles determined from neoclassical conductivity in a discharge with sawteeth. ρ_{inv} indicates the sawtooth inversion radius determined from an array of soft x-ray array detectors.

loop voltage profile is becoming spatially uniform, as it should be in equilibrium.

A large fraction of the current in this plasma is noninductive and is similar in magnitude to values predicted from bootstrap current and neutral beam current drive models. Figure 4(a) shows the current densities $J(\rho)$ and $J_{oh}(\rho)$ determined from neoclassical resistivity, indicating a relatively small level of inductive current. Figure 4(b) shows the noninductive current profile $J_{NI}(\rho)$ determined from the difference of $J(\rho)$ and $J_{oh}(\rho)$ and calculations of the bootstrap current and the sum of bootstrap and neutral beam driven current.[7,8] The estimation of the total noninductive current from the calculations is in general agreement with the exception of the central region which shows less beam driven current than the model predicts.

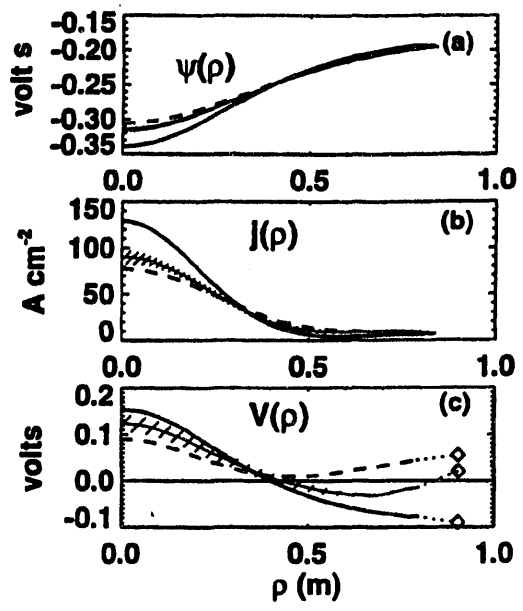

Fig. 3. Time evolving profiles of ψ, J, and $2\pi R_0 \mathcal{E}_{||}$ in a high-β_p plasma. Solid = 1.4 ss, solid + shading = 2.15 s, and dashed = 2.95 s. The shading for t = 2.15 s is representative of the uncertainty for the other times. The diamonds are the measured loop voltage on the vessel wall.

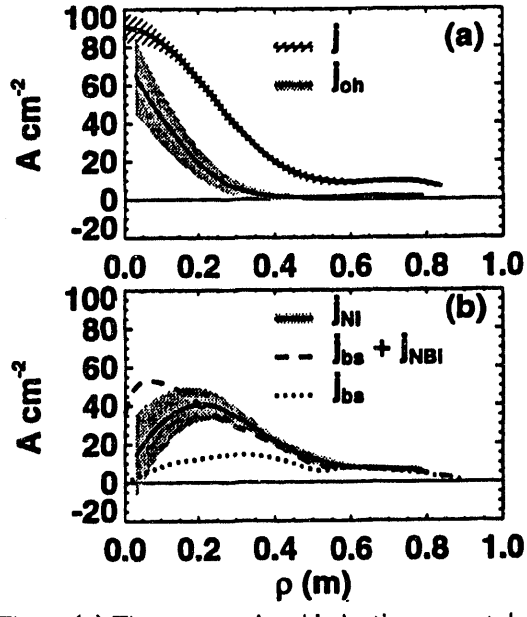

Fig. 4. (a) The measured and inductive current density, (b) noninductive current fraction determined from the difference from (a), and the calculated noninductive current due to neutral beam injection and bootstrap current, for the discharge of Fig. 3.

[1] D. Wroblewski and L.L. Lao, Rev. Sci. Instrum. **63**, 5140 (1992).

[2] F.L. Hinton and R.D. Hazeltine, Rev. Mod. Physics **48**, 239 (1976).

[3] L.L. Lao, J.R. Ferron, R.J. Groebner, W. Howl, H. St. John, E.J. Strait, and T.S. Taylor, Nucl. Fusion **30**, 1035 (1990).

[4] S.P. Hirshman and D.J. Sigmar, Nucl. Fusion **21**, 1079 (1981).

[5] K.H. Burrell, R.J. Groebner, T. Kurki-Suonio, T.N. Carlstrom, R.R. Dominguez, P. Gohil, R.A. Jong, H. Matsumoto, J.M. Lohr, T.W. Petrie, G.D. Porter, G.T. Sager, H. St. John, D.P. Schissel, S.M. Wolfe, and the DIII-D Research Group, in *Plasma Physics and Controlled Nuclear Fusion Research 1990*, Washington, DC (International Atomic Energy Agency, Vienna, 1991) p. 123.

[6] F. Alladio and G. Vlad, Phys. Fluids **31**, 602 (1988).

[7] S.P. Hirshman, Phys. Fluids **31**, 3150 (1988).

[8] J.D. Callen, R.J. Colcin, R.H. Fowler, D.G. McAlees, and J.A. Rome, in *Plasma Physics and Controlled Nuclear Fusion Research 1975*, Kyoto, Japan (International Atomic Energy Agency, Vienna, 1975) p. 645.

DATE
FILMED
10/4/94

END